Waveform Design With Interference Pre-cancellation Beyond Time-Reversal Systems

Yu-Han Yang, *Student Member, IEEE*, and K. J. Ray Liu, *Fellow, IEEE*

***Abstract*—In wideband communication systems, the time-reversal (TR) technique can boost the signal-to-noise ratio (SNR) at the receiver with simple single-tap detection. It has been shown that conventional waveform design can significantly improve the system performance of TR systems. However, when the symbol rate is very high, the severe intersymbol interference still limits the performance at high-power region. In this work, we study a new waveform design with interference pre-cancellation by exploiting the message information to further improve the performance. In the proposed design, the causal interference is subtracted by interference compensation, and the anticausal interference can be further suppressed by conventional waveform design by virtue of the more abundant degrees of freedom. The transmitter utilizes the information of previous symbols to enhance the signal quality while the receiver structure remains simple. In the multiuser scenario, both the interuser interference and intersymbol interference can be similarly categorized by the causality, and then be tackled accordingly by the proposed waveform design with interference pre-cancellation. The resulting multiuser waveform design is a nonconvex optimization problem, for which two iterative algorithms are proposed and both are guaranteed to converge to suboptimal solutions. Simulation results validate the convergence behavior and demonstrate the remarkable performance improvement over the conventional waveform design in the previous work.**

***Index Terms*—Interference cancellation, multi-user downlink, time-reversal, waveform design.**

I. Introduction

IN BASIC time-reversal (TR) communication systems [1], [2], the time-reversed channel impulse response serving as the transmit waveform is able to boost the signal strength in a large delay spread channel in broadband communication. After the transmitted TR waveform convolves with the multi-path channel, the temporal focusing effect [3], [4] of the TR waveform re-collects the most of signal energy into a single tap. Utilizing the channel reciprocity, such a time-reversed waveform is essentially a matched filter [5], which guarantees the optimal performance because of its capability of maximizing the signal-to-noise ratio (SNR). The TR transmission technique only requires a very low complexity at the receiver since a simple one-tap symbol estimation is performed. Thus, the TR transmission techniques have been shown to be a promising solution to the energy-efficient and low-complexity green wireless communication [1], [6].

In high speed wideband communication systems, however, when the symbol duration is smaller than the channel delay spread, the symbol waveforms are overlapped and thus interfere with each other. When the symbol rate is very high, the inter-symbol interference (ISI) can be notably severe and causes crucial performance degradation [7], [8]. Further, in multi-user downlink scenarios, the TR base-station uses each user's particular channel impulse response as the user's symbol waveform to modulate the symbols intended for that user. Despite the inherent randomness of the channel impulse responses, as long as they are not orthogonal to each other, which is almost always the case, these waveforms will inevitably interfere with each other when transmitted concurrently. Hence, the performance of TR transmission can be impaired and even limited by the inter-user interference (IUI). Moreover, interference can also be caused by incorporating multiple transmit antenna in the TR systems.

In a wideband environment, substantial degrees of freedom are available for the transmitted waveforms to be designed to combat the interference. Based on design criteria such as system performance, quality-of-service (QoS) constraints, or fairness among users, the waveform design can be formulated as an optimization problem with the transmitted waveforms as the optimization valuables. The basic idea of waveform design is to delicately adjust the amplitude and phase of each tap of the waveform based on the channel information, such that after convolving with the channel, the received signal at the receiver retains most of the intended signal strength and rejects or suppresses the interference as much as possible. It can be shown that the mathematical structure of waveform design is analogous to that of the precoder design in MISO systems, since the taps in waveform design act as the beamforming coefficients of the transmit antenna in the precoder design. In the literature, there have been many studies investigating the problems of designing advanced waveforms to suppress the interference [7]–[13]. In [7], a minimum mean-square-error (MMSE) waveform was proposed to suppress ISI and noise for a single-user scenario without taking into account the rate back-off factor in the optimization and thus the waveform is suboptimal. In [8], multi-user joint power allocation and waveform design for sum rate optimization was investigated in downlink TR systems. Different from the transmitter waveform design, in [14], an iterative soft-decision feedback equalization algorithm was introduced to combat the non-causal ISI created by the receiver matched filter.

Manuscript received June 16, 2015; revised December 23, 2015; accepted Janurary 25, 2016. Date of publication February 3, 2016; date of current version May 6, 2016. The associate editor coordinating the review of this paper and approving it for publication was W. Gerstacker.

The authors are with Origin Wireless, Inc., and the Department of Electrical and Computer Engineering, University of Maryland, College Park, MD 20742 USA (e-mail: yhyang@umd.edu; kjrliu@umd.edu).

Color versions of one or more of the figures in this paper are available online at http://ieeexplore.ieee.org.

Digital Object Identifier 10.1109/TWC.2016.2524526

Besides the channel information, another important side information the transmitter can exploit in the waveform design is the transmitted symbol information. Theoretically, if the receiver interference is known to the transmitter, it is possible to completely remove the interference by means of complicated coding techniques [15]. The interference is known to the transmitter since it can be derived from the transmit waveforms, the multipath channels, and the information bits. Given the transmitted symbols, the causal part of ISI can be compensated in advance in designing the waveform of the current symbol. Such a design is analogous to the transmitter-based interference pre-subtraction [16]–[20] in the nonlinear precoding literature. A substantial distinction for time-domain waveform design is that only the causal part of interference can be pre-canceled while the anti-causal part of interference cannot be compensated and needs to be suppressed by the waveform design based on the channel information. Note that throughout this paper, the term 'interference suppression' refers to linear waveform design as in [8], and the term 'interference pre-cancellation' corresponds to non-linear waveform design similar to the Tomlinson-Harashima Precoding (THP) [21], [22]. For MIMO systems, the causality restriction is in spatial domain, where the interference between antenna is canceled sequentially with a predetermined order. In this paper, the causality is considered in time domain, where the interference between information symbols is tackled sequentially according to the order they are transmitted. Note that in uplink scenarios, noncausal interference may also be estimated and compensated at the receiver since tentative decisions of detected symbols can be utilized to cancel the interference in the received signals [23].

In this work, we propose a waveform design with interference pre-cancellation for wideband communication systems such as TR systems. The single-user scenario permits a closed-form solution of the proposed waveform design. It is shown that the resulting design cancels the causal ISI and suppresses the anti-causal ISI. For the multi-user scenario, similarly the interference (both ISI and IUI) is categorized into causal interference and anti-causal interference. The interference-compensation filter design can be easily determined once the multi-user waveform design is settled. Since the resulting multi-user waveform design is non-convex, we propose two iterative algorithms to suboptimally tackle the optimization problem. One approach is based on the alternating optimization and the other is a gradient method [24]. We show that both iterative algorithms are guaranteed to converge to local optimal solutions. Numerical simulation is conducted to validate the convergence behavior of the proposed iterative algorithms and demonstrate the superior performance of the proposed waveform design.

A key distinction of this paper from previous work [8] is that the proposed waveform designs pre-cancels causal interference and suppresses anti-causal interference, while the waveform design in [8] suppresses both causal and anti-causal interference. The proposed algorithms not only can be applied in traditional time-reversal systems, where the receiver detects the transmitted information by a single tap, but can be easily extended to other systems where the receivers can deal with multi-tap detection. For example, the multiple taps can be combined into one tap using techniques such as maximum-ratio combining. The equivalent channel including the combining process can be similarly analyzed, and the proposed algorithms can be accordingly modified to be applied in such systems.

The contributions of this paper are summarized as follows.

- Time-domain causality is considered in transmitter waveform design for wideband communication systems such as TR systems. The interference between information symbols is pre-canceled sequentially according to the order they are transmitted. An essential observation is that only the causal part of interference can be pre-canceled while the anti-causal part of interference cannot be compensated and needs to be suppressed by the waveform design based on the channel information.
- For the multi-user scenario, the interference (both ISI and IUI) is categorized into causal interference and anti-causal interference. Similarly, the multi-user waveform design pre-cancels the causal interference and suppresses the anti-causal interference.
- Two iterative algorithms are proposed to tackle the non-convex multi-user waveform design problem. One approach is based on the alternating optimization and the other is a gradient method. Both iterative algorithms are guaranteed to converge and shown to have superior performance over other conventional designs.

The rest of the paper is organized as follows. In Section II, the system model of the TR communication system is introduced in detail. The waveform design with interference pre-cancellation for the single-user scenario is described in Section III, and the multi-user scenario is further depicted in Section IV, where the two iterative algorithms are proposed. In Section V, simulation results are shown to demonstrate the performance. Finally, we draw the conclusion in Section VI.

II. System Model

A multi-user downlink TR system consists of a base-station and K users. The multipath channel between the base-station and the k-th user is denoted by $\mathbf{h}_k$, a column vector of L elements where L is the maximum channel length among the K channels. Let s_k denote an information symbol and $\mathbf{g}_k$ be the transmit waveform for user k, which can be a basic TR waveform or a more advanced waveform [8]. The length of $\mathbf{g}_k$ is also L. As shown in Figure 1, the received signal $\mathbf{y}_k$ at user k is given by

$$\mathbf{y}_k = \mathbf{H}_k \sum_{j=1}^{K} \mathbf{g}_j s_j + \mathbf{n}_k, \tag{1}$$

where $\mathbf{H}_k$ is the Toeplitz matrix of size $(2L-1) \times L$ with the first column being $[\mathbf{h}_k^T \ \mathbf{0}_{1\times(L-1)}]^T$, and $\mathbf{n}_k$ denotes the additive white Gaussian noise (AWGN).

User k estimates the symbol s_k by scaling the sample $y_k[L]$ by α_k, which corresponds to the gain control at the receiver. Note that (1) represents the received signal when symbols are transmitted further apart, i.e., with a symbol rate being at most $1/L$ times sampling rate $1/T_s$. When the symbol rate is $1/(DT_s)$ where D denotes the rate back-off factor [7] and $D < L$, the received waveforms of different symbols overlap

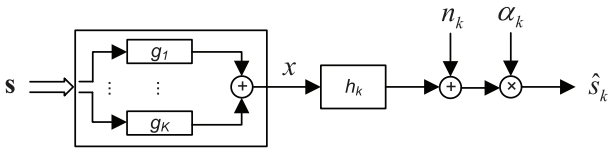

Fig. 1. Block diagram of waveform design for the multi-user downlink TR system.

with each other and give rise to the inter-symbol interference (ISI). Here D is the rate back-off factor introduced to adjust the symbol rate in TR systems [1], [2]. To characterize the effect of ISI, the decimated channel matrix of size $(2L_D - 1) \times L$, where $L_D = \lfloor \frac{L-1}{D} \rfloor + 1$, is defined as

$$\tilde{\mathbf{H}}_k = \sum_{i=-L_D+1}^{L_D-1} \mathbf{e}_{L_D+i} \mathbf{e}_{L+iD}^T \mathbf{H}_k, \tag{2}$$

where $\mathbf{e}_l$ is the l-th column of a $(2L - 1) \times (2L - 1)$ identity matrix. In other words, $\tilde{\mathbf{H}}_k$ is obtained by decimating the rows of $\mathbf{H}_k$ by D, i.e., centering at the L-th row, every D-th row of $\mathbf{H}_k$ is kept in $\tilde{\mathbf{H}}_k$ while the other rows are discarded. The decimated channel takes into consideration only the samples of interest and forcing everything else to zero. The center row index of $\tilde{\mathbf{H}}_k$ is L_D. Then the sample for symbol estimation can be written as

$$\begin{aligned} y_k[L] = \mathbf{h}_{kL_D}^H \mathbf{g}_k s_k[L_D] + \mathbf{h}_{kL_D}^H \sum_{j \neq k} \mathbf{g}_j s_j[L_D] \\ + \sum_{l=1, l \neq L_D}^{2L_D-1} \mathbf{h}_{kl}^H \sum_{j=1}^{K} \mathbf{g}_j s_j[l] + n_k[L], \end{aligned} \tag{3}$$

where the $\mathbf{h}_{kl}^H = \mathbf{e}_l^T \tilde{\mathbf{H}}_k$ denotes the l-th row of $\tilde{\mathbf{H}}_k$, and $s_j[l]$ denotes user j's l-th symbol. It can be seen from [3] that the symbol $s_k[L_D]$, the L_D-th symbol of user k, is interfered by the previous $L_D - 1$ symbols and the later $L_D - 1$ symbols as well as other users' $K(2L_D - 1)$ symbols, and also corrupted by the noise. The design of waveforms $\{\mathbf{g}_k\}$ has critical influence to the symbol estimation and thus the system performance. If the basic TR waveforms are adopted, i.e., $\mathbf{g}_k = \mathbf{h}_{kL}$, then the intended signal power for each user is maximized but without considering the interference caused by other symbols. As such, the performance is limited by the interference when the transmit power is high. Another possible waveform design is zero-forcing (ZF) [25], which minimizes all the interference signal power but without taking into account the intended signal power. Thus, the resulting SNR can be very low and causes severe performance degradation especially when the transmit power is relatively low. In our previous work [8], it has been shown that well-designed waveforms can strike a balance between enhancing the intended signal power and suppressing the interference power.

III. Single-User Waveform Design With Interference Pre-Cancellation

In this section, we discuss the waveform design with interference pre-cancellation for the single-user case, which allows a closed form solution and provides an insight to the proposed design in the multi-user scenario. To simplify the notations, the user index for the single-user scenario is omitted. For example, the channel, the waveform, and the gain are denoted as $\mathbf{h}$, $\mathbf{g}$, and α, respectively. In [8], a waveform design is proposed to suppress the ISI by designing the transmit waveform $\mathbf{g}$ based on the criterion of maximizing the signal-to-interference-plus-noise ratio (SINR). Such a formulation usually involves solving an eigenvalue problem. In this paper, we consider minimizing mean-square error (MSE) as the design criterion. It can be shown that in the single-user case, a closed form solution to the proposed design can be derived, and the minimum MSE waveform without interference pre-cancellation also achieves the maximum SINR [8], [26]. Minimizing MSE is equivalent to maximizing SINR for single-user scenarios, in the sense that the resulting waveform design and the system error probability performance are the same. A minor difference of the two approaches is the route of computation. For maximizing SINR, the problem formulation leads to solving an eigensystem, where the eigenvector represents the waveform and the eigenvalue relates to the maximum SINR. For minimizing MSE, a closed-form solution can be given as described later in this subsection. In the following, we will first discuss the waveform design for minimizing MSE without interference pre-cancellation, and then the interference-compensation filter design. Finally, the waveform design with interference pre-cancellation is analyzed and the closed form solution is derived.

A. Waveform Design Without Interference Pre-Cancellation

The estimated symbol is obtained by scaling the sample $y[L]$ by the gain α, i.e., $\hat{s}[L_D] = \alpha y[L]$. Let the l-th row of the decimated channel matrix $\tilde{\mathbf{H}}$ be denoted by $\mathbf{h}_l^H$. The estimation MSE defined as $E[\|\hat{s}[L_D] - s[L_D]\|^2]$ is expressed as

$$\begin{aligned} \mathrm{MSE}(\alpha, \mathbf{g}) = |\alpha \mathbf{h}_{L_D}^H \mathbf{g} - 1|^2 P_S + \sum_{l=1, l \neq L_D}^{2L_D-1} |\alpha \mathbf{h}_l^H \mathbf{g}|^2 P_S \\ + |\alpha|^2 P_N, \end{aligned} \tag{4}$$

where $s[l], l = 1, \ldots, L_D - 1, L_D + 1, \ldots, 2L_D - 1$, denote the interfering symbols transmitted adjacent to the intended symbol $s[L_D]$. The symbol power $P_S = E[|s[l]|^2]$, $\forall l$, is assumed to be unity for normalization. The noise is i.i.d. Gaussian distributed and hence $P_N = E[|n[l]|^2]$, $\forall l$.

The minimum MSE (MMSE) waveform $\mathbf{g}$ can be derived by formulating the problem as minimizing MSE subject to a power constraint $\mathbf{g}^H \mathbf{g} = P_{\max}$ to rule out the trivial solution $\mathbf{g} = \mathbf{0}$, the all-zero vector.

The optimal gain α^{SU} can be shown to be

$$\alpha^{\mathrm{SU}} = \sqrt{P_{\max}^{-1} \mathbf{h}_{L_D}^H \left(\sum_{l=1}^{2L_D-1} \mathbf{h}_l \mathbf{h}_l^H + \frac{P_N}{P_{\max}} \mathbf{I} \right)^{-2} \mathbf{h}_{L_D}}, \tag{5}$$

where the superscript SU denotes the single-user scenario. The optimal waveform can be obtained as

$$\mathbf{g}^{\mathrm{SU}} = \alpha^{\mathrm{SU}-1} \left(\sum_{l=1}^{2L_D-1} \mathbf{h}_l \mathbf{h}_l^H + \frac{P_N}{P_{\max}} \mathbf{I} \right)^{-1} \mathbf{h}_{L_D}. \tag{6}$$

The resulting minimum MSE in the TR system is given by

$$\mathrm{MSE}^{\mathrm{SU}} = 1 - \mathbf{h}_{L_D}^H \left(\sum_{l=1}^{2L_D-1} \mathbf{h}_l \mathbf{h}_l^H + \frac{P_N}{P_{\max}} \mathbf{I} \right)^{-1} \mathbf{h}_{L_D}. \quad (7)$$

Note that the phase of α can be chosen arbitrarily without altering the MSE. Therefore, we choose a real-valued α^{SU} as in (5). From the derivation above, we can obtain the closed-form solution to the waveform design without interference pre-cancellation given the channel matrix and the signal power to noise power ratio.

The computational complexity of inverting the matrix in (6) depends on the decimation factor D. When $D = 1$, the matrix can be shown to be Toeplitz. Inverting a Toeplitz matrix can be accomplished in $O(L^2)$ using Trench's algorithm [27]. For general D, the matrix is periodic Toeplitz, whose inversion can be solved by Levinson's algorithm [28] in $O(L^2 D)$. Another algorithm for general D is to recursively apply the matrix inversion lemma and solve the inversion in $O(L^2 \lfloor \frac{L}{D} \rfloor)$. Define

$$\mathbf{R}_m^{-1} = \left(\sum_{l=1}^{m} \mathbf{h}_l \mathbf{h}_l^H + \frac{P_N}{P_{\max}} \mathbf{I} \right)^{-1}. \quad (8)$$

Applying the matrix inversion lemma, we have

$$\begin{aligned} \mathbf{R}_m^{-1} &= \left(\mathbf{h}_m \mathbf{h}_m^H + \mathbf{R}_{m-1} \right)^{-1} \\ &= \mathbf{R}_{m-1}^{-1} - \left(1 + \mathbf{h}_m^H \mathbf{R}_{m-1}^{-1} \mathbf{h}_m \right)^{-1} \mathbf{R}_{m-1}^{-1} \mathbf{h}_m \mathbf{h}_m^H \mathbf{R}_{m-1}^{-1}. \end{aligned} \quad (9)$$

Given $\mathbf{R}_{m-1}^{-1}$ and $\mathbf{h}_m$, equation (9) can be computed in $O(L^2)$. By sequentially calculating $\mathbf{R}_m^{-1}$ for $m = 1, 2, \ldots, 2L_D - 1$ using (9), the matrix inversion $\mathbf{R}_{2L_D-1}^{-1}$ can be obtained in $O(L^2 \lfloor \frac{L}{D} \rfloor)$.

Therefore, Levinson's algorithm can be applied when D is small, and the recursive matrix inversion algorithm can be used when D is large. Consequently, the computational complexity of the matrix inversion in (6) is $O(\min(L^2 D, L^2 \lfloor \frac{L}{D} \rfloor)) = O(L^{2.5})$.

B. Interference Pre-Cancellation

In TR systems, a user estimates the intended symbol by the sample of the central peak of the receive signal. Therefore, the ISI can be identified as two parts: the causal ISI and the anti-causal ISI. Due to the overlapping of the received signals of consecutive symbols, one symbol can have influence to the *previous* transmitted symbols and also to the *future* transmitted symbols. To compensate for the interference caused by the previous symbols, the current symbol can be subtracted by the interference before convolving with the transmit waveform. Let $v[k]$ denote the input to the transmit waveform $\mathbf{g}$ after the interference compensation, that is,

$$v[k] = s[k] - (\mathbf{h}_{L_D}^H \mathbf{g})^{-1} \sum_{l=1}^{L_D-1} (\mathbf{h}_{L_D+l}^H \mathbf{g}) v[k-l]. \quad (10)$$

The operation in (10) can be considered as passing the symbols $s[\cdot]$ through a feedback filter $\mathbf{b}^{\mathrm{ZF}} = (\mathbf{h}_{L_D}^H \mathbf{g})^{-1} [\mathbf{0}_{1\times L_D}, -\mathbf{h}_{L_D+1}^H \mathbf{g}, \ldots, -\mathbf{h}_{2L_D-1}^H \mathbf{g}]$, where $\mathbf{0}_{1\times L_D}$ denotes a $1 \times L_D$ zero vector. The resulting MSE is then given by

$$\mathrm{MSE}^{\mathrm{IM}} = |\alpha \mathbf{h}_{L_D}^H \mathbf{g} - 1|^2 P_V + \sum_{l=1}^{L_D-1} |\alpha \mathbf{h}_l^H \mathbf{g}|^2 P_V + |\alpha|^2 P_N, \quad (11)$$

where P_V, the average power of $v[\cdot]$, usually requires more power than P_S since additional power is needed for the second term in (10) even though the causal interference part $\sum_{l=L_D+1}^{2L_D-1} |\alpha \mathbf{h}_l^H \mathbf{g}|^2$ can be completely compensated. Thus, the benefit of performing interference pre-cancellation can be impaired by the performance degradation caused by the additional power. Especially when the noise power is more dominant than the interference power, the interference pre-cancellation cannot provide much performance improvement and much of the transmit power would be wasted in performing the interference pre-cancellation.

The problem of the increase of the transmit power can be resolved by applying the Tomlinson-Harashima Precoding (THP) [21], [22], which is to incorporate a modulo-A component after the interference pre-cancellation at the transmitter, and a modulo-A component before the symbol estimation at the receiver. This technique is able to address the additional transmit power problem in (10) because the modulo-A operation at the transmitter folds the signal constellation into $[-\frac{A}{2}, \frac{A}{2})$, and thus the average power is limited within the range regardless of the interference power. The resulting block diagram is depicted in Figure 2(a). The modulo-A operation, denoted as $\mathrm{mod}_A(\cdot)$, is to subtract element-wise the nearest integral multiple of A from the input such that each element of the output is in $[-\frac{A}{2}, \frac{A}{2})$, i.e., for an input v,

$$\mathrm{mod}_A(v) = v - A \left\lfloor \frac{v}{A} + \frac{1}{2} \right\rfloor, \quad (12)$$

where $\lfloor \cdot \rfloor$ is the floor operator, which returns the highest integer that is lower or equal to the input value. Note that for complex value, the modulo-A operator applies to both the real and the imaginary parts independently. With different constellation size of the symbol modulation (e.g., QPSK, 16-QAM, or 64-QAM), the parameter A can be chosen accordingly to minimize the modulo loss which will be explained in detail in Section III-D.

C. Waveform Design With Interference Pre-Cancellation

The modulo-A component imposes nonlinearity to the design of the feedback filter $\mathbf{b}$. The nonlinear part can be moved to the outermost of the system design such that the converted system in Figure 2(b) is equivalent to the original system in Figure 2(a), [29]–[31], where a and a' denote integral multiples of A such that the outputs of the modulo components are within the proper range. We can focus on minimizing the MSE of the linear part of the system, i.e., $\mathrm{MSE}^{\mathrm{IM}} = E[\|\hat{u} - u\|^2]$, where the superscript IM denotes interference pre-cancellation, u denotes the

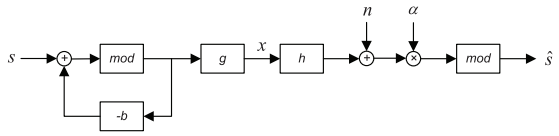

(a) Block diagram of waveform design with interference pre-cancellation for a single-user TR system.

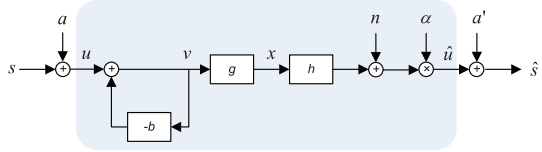

(b) Equivalent block diagram of (a).

Fig. 2. Block diagrams of waveform design with interference pre-cancellation for a single-user TR system.

symbol after adding a to the original input s, and $\hat{u}$ is the symbol before adding a' for the estimated symbol $\hat{s}$. The MSE is given by

$$\begin{aligned}\mathrm{MSE}^{\mathrm{IM}}(\mathbf{g},\mathbf{b},\alpha) = &\\ &|\alpha|^2 \sum_{l=1}^{L_D-1} |\mathbf{h}_l^H \mathbf{g}|^2 P_V + |\alpha \mathbf{h}_{L_D}^H \mathbf{g} - 1|^2 P_V \\ &+ \sum_{l=L_D+1}^{2L_D-1} |\alpha \mathbf{h}_l^H \mathbf{g} - b[l]|^2 P_V + |\alpha|^2 P_N, \quad (13)\end{aligned}$$

where P_V is the average power of the modulo output. The first term, $|\alpha|^2 \sum_{l=1}^{L_D-1} |\mathbf{h}_l^H \mathbf{g}|^2 P_V$, is the anti-causal interference caused by the symbols transmitted after the current symbol. The third term, $\sum_{l=L_D+1}^{2L_D-1} |\alpha \mathbf{h}_l^H \mathbf{g} - b[l]|^2 P_V$, is the causal interference caused by the symbols transmitted before the current symbol. Our goal of the waveform design with interference pre-cancellation is to jointly determine the parameters $\mathbf{b}$, $\mathbf{g}$ and α such that the MSE is minimized. It is clear that the optimal $b[l]$ should be chosen such that

$$b[l] = \begin{cases} \alpha \mathbf{h}_l^H \mathbf{g}, & l = L_D+1, \ldots, 2L_D-1, \\ 0, & \text{otherwise.} \end{cases} \quad (14)$$

Substituting (14) into (13) and setting $P_V = 1$ for normalization, we can solve the problem of MSE minimization subject to a transmit power constraint by a similar analysis as in the derivation for (5). The optimal α and $\mathbf{g}$ are given by

$$\alpha^{\mathrm{IM}} = \sqrt{P_{\max}^{-1} \mathbf{h}_{L_D}^H \left(\sum_{l=1}^{L_D-1} \mathbf{h}_l \mathbf{h}_l^H + \frac{P_N}{P_{\max}} \mathbf{I} \right)^{-2} \mathbf{h}_{L_D}}, \quad (15)$$

$$\mathbf{g}^{\mathrm{IM}} = \alpha^{-1} \left(\sum_{l=1}^{L_D-1} \mathbf{h}_l \mathbf{h}_l^H + \frac{P_N}{P_{\max}} \mathbf{I} \right)^{-1} \mathbf{h}_{L_D} \quad (16)$$

The resulting minimum MSE is given by

$$\mathrm{MSE}^{\mathrm{IM}} = 1 - \mathbf{h}_{L_D}^H \left(\sum_{l=1}^{L_D-1} \mathbf{h}_l \mathbf{h}_l^H + \frac{P_N}{P_{\max}} \mathbf{I} \right)^{-1} \mathbf{h}_{L_D}. \quad (17)$$

Examining the difference between (6) and (16), we can see that $\mathbf{g}^{\mathrm{IM}}$ takes into account only the anti-causal ISI, which comprises the 1st to the (L_D-1)-th rows of the decimated channel matrix $\tilde{\mathbf{H}}$. The causal ISI, i.e., the (L_D+1)-th to the $(2L_D-1)$-th rows, are not considered in $\mathbf{g}^{\mathrm{IM}}$ since they can be compensated by the feedback filter $\mathbf{b}$. The difference between the resulting MMSEs in (7) and (17) also demonstrates such an effect.

The design of the optimal parameters can be summarized as follows. First, the receiver gain α^{IM} is determined by (15). Then the waveform $\mathbf{g}^{\mathrm{IM}}$ is designed to suppress the anti-causal interference using (16) given α^{IM}. Finally, the coefficients of the feedback filter $\mathbf{b}$ for interference pre-cancellation is obtained by [14] given $\mathbf{g}^{\mathrm{IM}}$ and α^{IM}. Note that the calculation is performed at the transmitter and at the decoding process the receiver needs to compute the parameter α^{IM} based on

$$\alpha^{\mathrm{IM}} = \frac{(\mathbf{h}_{L_D}^H \mathbf{g}^{\mathrm{IM}})^*}{\sum_{l=1}^{L_D} |\mathbf{h}_l^H \mathbf{g}^{\mathrm{IM}}|^2 + P_N/P_V}, \quad (18)$$

which is derived by minimizing (13). The knowledge of the equivalent channel coefficients, $\mathbf{h}_l^H \mathbf{g}^{\mathrm{IM}}, \forall l$, could be acquired by channel estimation using a known training sequence. For multi-user scenario, the equivalent channel estimation can be similarly done by each user.

D. Bit Error Rate Analysis

The performance of the waveform design with interference pre-cancellation can be analyzed by considering several losses of incorporating the THP, including power loss, modulo loss, and shaping loss [32], [33]. The power loss is due to the fact that the modulo output still requires higher power P_V than the symbol power P_S. Since the modulo operation changes the constellation to be repeated over the whole space and such a change shrinks the decision region of those symbols at the boundary of the constellation, when those boundary symbols are transmitted, the received symbols may be misinterpreted as wrong symbols and modulo loss occurs. Finally, the shaping loss happens when the distribution of the transmit signal becomes non-Gaussian since information-theoretically the optimal input distribution is Gaussian while the modulo operation generally produces a uniform distributed signal. The output of the modulo operation is passed though the transmit waveform, which considerably randomizes the distribution and tends to give rise to a Gaussian-like distribution based on the observation in our numerical simulations. Hence, in the following analysis, we neglect the shaping loss and focus on the power loss and modulo loss.

The output of the modulo operation is uniformly distributed when the interference to be compensated is large enough. Considering both in-phase and quadrature components of $v[\cdot]$, we can have $P_V = \frac{A^2}{6}$, where A is the modulo operation size. The optimal choice of A depends on the constellation size [34]. For example, $A = 2\sqrt{2}$ for QPSK and the power loss is $4/3 \approx 1.25$ dB. As discussed above, the modulo loss occurs when the boundary symbols are transmitted, and thus depends

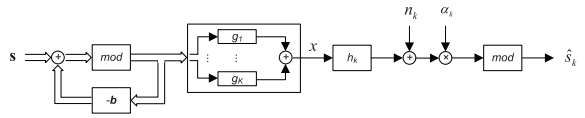

(a) Block diagram of waveform design with interference pre-cancellation for a multi-user TR system.

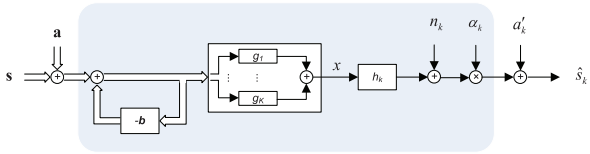

(b) Equivalent block diagram of (a).

Fig. 3. Block diagrams of waveform design with interference pre-cancellation for a multi-user TR system.

on the constellation size. The bit error rate for QPSK can be approximated by [35]

$$P_b^{\text{QPSK}} \approx 2Q\left(\sqrt{\frac{\frac{1}{2}P_S}{P_{\text{ISI}}+\sigma^2}}\right) - 2Q\left(3\sqrt{\frac{\frac{1}{2}P_S}{P_{\text{ISI}}+\sigma^2}}\right) + 2Q\left(5\sqrt{\frac{\frac{1}{2}P_S}{P_{\text{ISI}}+\sigma^2}}\right) - \ldots, \tag{19}$$

where $P_{\text{ISI}} = P_V \sum_{l=1}^{L_D-1} |\mathbf{h}_l^H \mathbf{g}|^2$. For higher order constellation such as 16-QAM or 64-QAM, the analysis can be derived similarly.

IV. Multi-User Waveform Design With Interference Pre-Cancellation

In the waveform design with interference pre-cancellation for the single-user TR system, the causal ISI is compensated by the feedback filter and anti-causal ISI is suppressed by the waveform design. In the multi-user downlink TR system, we can leverage a similar idea of compensating both the causal ISI and the causal IUI by feedback filters, and suppressing both the anti-causal ISI and the anti-causal IUI by the multi-user waveform design.

Figure 3(a) depicts the block diagram of a multi-user TR system with interference pre-cancellation. The wide arrows denote the flow of a vector of data streams as the extension of Figure 2. The feedback filter takes a vectored input and turns out a vectored output. In the waveform part, each data stream is convolved with its waveform $\mathbf{g}_k$ and the outputs are additively aggregated together to be the transmit signal.

To determine the causality of IUI and ISI, the ordering of users for interference pre-cancellation has to be settled. Notice that all users' signals are transmitted simultaneously and the causality of users is determined by the ordering of IUI compensation. Finding the optimal ordering requires exhaustive search over all possible permutations and is computationally prohibitive. Moreover, as will be shown in Section V, the overhead of searching may not be worthy since the amount of interference with different orderings differs only in the current symbols, which contribute a relatively small portion

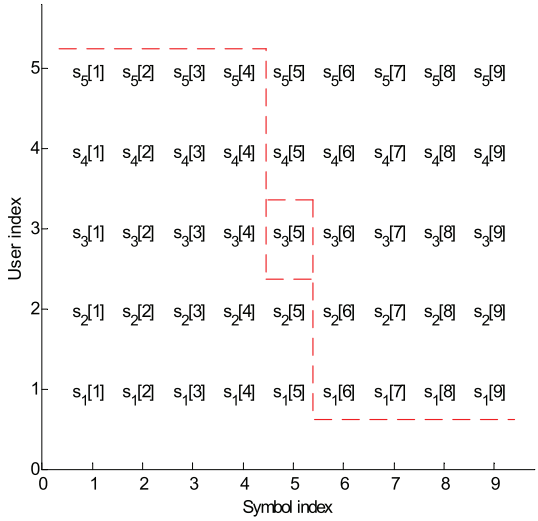

Fig. 4. Illustration of the causality of interference caused by symbols of users.

to the overall interference. In the following, we denote the index of a user as its ordering. For user k's L_D-th symbol, $s_k[L_D]$, the causal interference is caused by the symbols including $\{s_j[l], l < L_D, \forall j\}$ and $\{s_j[L_D], j < k\}$; the anti-causal interference is caused by the symbols $\{s_j[l], l > L_D, \forall j\}$ and $\{s_j[L_D], j > k\}$. Figure 4 illustrates the causality of interference for a multi-user system with $K = 5$ and $L_D = 5$, and different causalities are separated by dash lines. When the current symbol is $s_3[5]$, the symbols in the bottom left part of Figure 4 serve as the causal interference to be compensated by the feedback filter, and the symbols in the top right part of Figure 4 are the anti-causal interference to be suppressed by the waveform design.

Similar to the single-user case, we consider the linear part of the equivalent system in Figure 3(b). The MSE of user k in can be expressed as

$$\begin{aligned}\text{MSE}_k = &\sum_{j=1}^{K}\sum_{l=1}^{L_D-1} |\alpha_k \mathbf{h}_{kl}^H \mathbf{g}_j|^2 P_V + \sum_{j>k} |\alpha_k \mathbf{h}_{kL_D}^H \mathbf{g}_j|^2 P_V \\ &+ |\alpha_k \mathbf{h}_{kL_D}^H \mathbf{g}_k - 1|^2 P_V \\ &+ \sum_{j<k} |\alpha_k \mathbf{h}_{kL_D}^H \mathbf{g}_j - b_{kj}[L_D]|^2 P_V \\ &+ \sum_{j=1}^{K}\sum_{l=1}^{L_D-1} |\alpha_k \mathbf{h}_{kl}^H \mathbf{g}_j - b_{kj}[l]|^2 P_V + |\alpha_k|^2 P_N, \end{aligned} \tag{20}$$

where $b_{kj}[\cdot]$ denotes the feedback filter of user k for compensating for the interference of user j's data stream. In the following, we aim to jointly design the waveforms $\{\mathbf{g}_k\}$, the feedback filters $\{\mathbf{b}_k\}$, and the gains $\{\alpha_k\}$ such that the total MSE is minimized. It is clear that the optimal coefficients of the feedback filter are given by

$$b_{kj}[l] = \begin{cases} \alpha_k \mathbf{h}_{kl}^H \mathbf{g}_j, & l = L_D+1, \ldots, 2L_D-1, \forall j, \\ & \text{or } l = L_D, j < k, \\ 0, & \text{otherwise.} \end{cases} \tag{21}$$

Substituting [21] into (20), we have

$$\mathrm{MSE}_k = \sum_{j=1}^{K}\sum_{l=1}^{L_D-1} |\alpha_k \mathbf{h}_{kl}^H \mathbf{g}_j|^2 P_V + \sum_{j>k} |\alpha_k \mathbf{h}_{kL_D}^H \mathbf{g}_j|^2 P_V + |\alpha_k \mathbf{h}_{kL_D}^H \mathbf{g}_k - 1|^2 P_V + |\alpha_k|^2 P_N. \quad (22)$$

It can be seen that user k's optimal waveform $\mathbf{g}_k$ relies on other users' optimal waveforms. Therefore, unlike the single-user case, the closed form global optimal solution of the multi-user problem is difficult to find. Hence, we propose two iterative algorithms to search for locally optimal solutions. One approach is an alternating optimization method and the other is a gradient method. The convergence of both iterative algorithms can be guaranteed by showing the monotonicity of the objective functions during the iterations.

A. Alternating Optimization Algorithm

The alternating optimization algorithm is to iteratively optimize over a restricted subset of all variables [24]. In this proposed algorithm, we iteratively update the waveforms $\{\mathbf{g}_k\}$ and the gains $\{\alpha_k\}$ to optimize the total MSE subject to a power constraint. It will be shown that fixing one set of variables, optimization over the other set of variables is a convex problem and the closed-form solution can be derived. The total MSE in each iteration is non-increasing and thus the alternating optimization algorithm is guaranteed to converge.

It is easy to optimize the gains $\{\alpha_k\}$ given a set of fixed waveforms $\{\mathbf{g}_k\}$ since the total MSE $\sum_{k=1}^{K} \mathrm{MSE}_k$ is a quadratic function of $\{\alpha_k\}$. We can consider the first order condition, i.e., the first order derivative of the total MSE with respect to α_k equals zero. We can have

$$\alpha_k = \left(\sum_{j\geq k} |\mathbf{h}_{kL_D}^H \mathbf{g}_j|^2 + \sum_{j=1}^{K}\sum_{l=1}^{L_D-1} |\mathbf{h}_{kl}^H \mathbf{g}_j|^2 + \frac{P_N}{P_V}\right)^{-1} \cdot \mathbf{g}_k^H \mathbf{h}_{kL_D}, \quad \forall k. \quad (23)$$

Next, we consider the optimization of the waveforms $\{\mathbf{g}_k\}$ subject to a power constraint, with a set of fixed gains $\{\alpha_k\}$. Directly taking the derivative of the Lagrangian with respect to $\{\mathbf{g}_k\}$ leads to an expression in terms of the Lagrange multiplier λ associated with the power constraint. Solving λ, however, is quite difficult and arouses the need for numerical search. Motivated by the technique in solving (6) where the Lagrange multiplier can be explicitly obtained, we propose to keep the ratio between $\{\alpha_k\}$ fixed and optimize the corresponding $\{\mathbf{g}_k\}$ so that the Lagrange multiplier can be solved explicitly. That is, instead of fixing $\{\alpha_k\}$, we fix $\bar{\alpha}_k = \gamma^{-1}\alpha_k$, for all k, where $\gamma = \sqrt{\sum_k |\alpha_k|^2 / P_{\max}}$, which means $\sum_k |\bar{\alpha}_k|^2 = P_{\max}$, and γ is considered as a variable in the optimization problem. The Lagrangian of minimizing the total MSE subject to the power constraint, with variables γ and $\mathbf{g}_k, \forall k$, is given by

$$\mathcal{L}(\mathbf{g}_1, ..., \mathbf{g}_K, \gamma, \lambda) = \sum_{k=1}^{K} \mathrm{MSE}_k + \lambda\left(\sum_{k=1}^{K} \mathbf{g}_k^H \mathbf{g}_k - P_{\max}\right). \quad (24)$$

TABLE I
ALTERNATING OPTIMIZATION ALGORITHM FOR MULTI-USER DOWNLINK WAVEFORM DESIGN

(i) Initialize $\alpha_k = 1, \forall k$.
(ii) **Loop** :
1. *Calculate waveforms*: $\{\mathbf{g}_k\}$ and γ by (25) and (26).
2. *Calculate gains*: $\{\alpha_k\}$ by (23).

Until α_k, $\{\mathbf{g}_k\}$ and γ converge or the max. number of iterations is reached.

Taking the first order derivative of $\mathcal{L}$ with respect to $\mathbf{g}_k^*$, we have

$$\mathbf{g}_k = \gamma^{-1}\bar{\alpha}_k^* \left(\sum_{j\leq k} |\bar{\alpha}_j|^2 \mathbf{h}_{jL_D}\mathbf{h}_{jL_D}^H + \sum_{j=1}^{K}\sum_{l=1}^{L_D-1} |\bar{\alpha}_j|^2 \mathbf{h}_{jl}\mathbf{h}_{jl}^H + \frac{\lambda}{P_V}\mathbf{I}\right)^{-1} \mathbf{h}_{kL_D}. \quad (25)$$

Taking the first order derivative of $\mathcal{L}$ with respect to γ, we have

$$\gamma = \left(\sum_{k=1}^{K} \bar{\alpha}_k^* \mathbf{g}_k^H \mathbf{h}_{kL_D}\right)\left(\sum_{k=1}^{K}\left(\sum_{j\leq k} |\bar{\alpha}_j \mathbf{h}_{jL_D}^H \mathbf{g}_k|^2 + \sum_{j=1}^{K}\sum_{l=1}^{L_D-1} |\bar{\alpha}_j \mathbf{h}_{jl}^H \mathbf{g}_k|^2 + \frac{P_N}{P_V}|\bar{\alpha}_k|^2\right)\right)^{-1}. \quad (26)$$

From (25), (26), and the power constraint $\sum_k \mathbf{g}_k^H \mathbf{g}_k = P_{\max}$, we can have $\lambda = P_N$. By substituting γ and $\lambda = P_N$ into (25), the closed form solution of $\mathbf{g}_k$ can be obtained.

The proposed alternating optimization algorithm, summarized in Table I, is to fix one set of variables and optimize the other set of variables to decrease the total MSE until convergence or the maximum number of iterations is reached. When the waveforms $\{\mathbf{g}_k\}$ are fixed, updating the gains $\{\alpha_k\}$ can only reduce the total MSE or keep it unchanged. Similarly, when the normalized gains $\{\bar{\alpha}_k\}$ are fixed, updating the waveforms $\{\mathbf{g}_k\}$ also makes the total MSE non-increasing. Thus, it can be easily seen that the proposed alternating optimization algorithm always converges since the total MSE is always non-increasing during the iterations and the total MSE is lower bounded by zero. Note that the converged solution may not be a globally optimal solution but it is a local optimum where none of the two optimization steps can further improve the performance.

B. Gradient Algorithm

The gradient method, by iteratively updating the variables to the steepest direction that decreases the objective function, is able to locate the global minimum for convex functions, but only a local optimum for a wide class of non-convex functions [24]. We propose to remove the dependence of $\{\alpha_k\}$ by substitute (23) into the MSE in (22) so that the gradient method can

TABLE II
GRADIENT ALGORITHM FOR MULTI-USER DOWNLINK WAVEFORM DESIGN

(i) Initialize $\mathbf{g}_k = \mathbf{h}_{kL_D}, \forall k, d = 1$.
(ii) **Loop**:
(a) *Calculate gradients*: $\{\Delta \mathbf{g}_k\}$ by (29).
(b) *Update waveforms*: $\{\mathbf{g}_k^{(n)}\}$ by (30).
(c) *Line search*:
If $\sum_k \text{MSE}_k^{(n)} > \sum_k \text{MSE}_k^{(n-1)}$
$d = d + 1$, $\delta^{(n)} = \frac{1}{d}$.
goto (b).
else
$n = n + 1$.
end if
Until $\{\mathbf{g}_k\}$ converge or the max. number of iterations is reached.

focus on updating $\{\mathbf{g}_k\}$ only. Then the resulting total MSE as a function of $\{\mathbf{g}_k\}$ is given by

$$\sum_{k=1}^{K} \text{MSE}_k = P_V \sum_{k=1}^{K} \left(1 - t_k^{-1} |\mathbf{g}_k^H \mathbf{h}_{kL_D}|^2\right), \tag{27}$$

where

$$t_k = \sum_{j \geq k} |\mathbf{h}_{kL_D}^H \mathbf{g}_j|^2 + \sum_{j=1}^{K} \sum_{l=1}^{L_D - 1} |\mathbf{h}_{kl}^H \mathbf{g}_j|^2 + \frac{P_N}{P_V}. \tag{28}$$

It can be easily verified that the total MSE in (27) is non-convex in $\{\mathbf{g}_k\}$. The gradient of $\mathbf{g}_k$ can be obtained as

$$\begin{aligned} \Delta \mathbf{g}_k &\triangleq \frac{\partial}{\partial \mathbf{g}_k^*} \left(\sum_k \text{MSE}_k \right) \\ &= P_V \left(-\mathbf{h}_{kL_D} \mathbf{h}_{kL_D}^H t_k^{-1} + \sum_{j=1}^{k} |\mathbf{g}_j^H \mathbf{h}_{jL_D}|^2 \mathbf{h}_{jL_D} \mathbf{h}_{jL_D}^H t_j^{-2} \right. \\ &\quad \left. + \sum_{j=1}^{K} \sum_{l=1}^{L_D - 1} |\mathbf{g}_j^H \mathbf{h}_{jL_D}|^2 \mathbf{h}_{jl} \mathbf{h}_{jl}^H t_j^{-2} \right) \mathbf{g}_k. \end{aligned} \tag{29}$$

The gradient algorithm is summarized in Table II, where the waveforms are iteratively updated by

$$\mathbf{g}_k^{(n+1)} = \text{proj}_{\mathcal{C}} \left[\mathbf{g}_k^{(n)} - \delta^{(n)} \frac{\Delta \mathbf{g}_k^{(n)}}{\| \Delta \mathbf{g}_k^{(n)} \|_2} \right]. \tag{30}$$

We choose the step size $\delta^{(n)}$ to be the harmonic sequence $\frac{1}{d}, d = 1, 2, \ldots$ for its good convergence behavior [24]. The projection operator $\text{proj}_{\mathcal{C}}$ is to project the updated waveforms into the constraint set $\sum_{k=1}^{K} \mathbf{g}_k^H \mathbf{g}_k = P_{\max}$ by normalization. Note that by choosing a proper step size as described by the line search in Table II, the update in (30) is guaranteed to reduce the total MSE.

In each iteration, the total MSE generated by the proposed gradient algorithm is non-increasing. By the same argument that the sequence of the total MSE is non-increasing and bounded below, the proposed gradient algorithm is guaranteed to converge to a local minimum, where the gradient is zero.

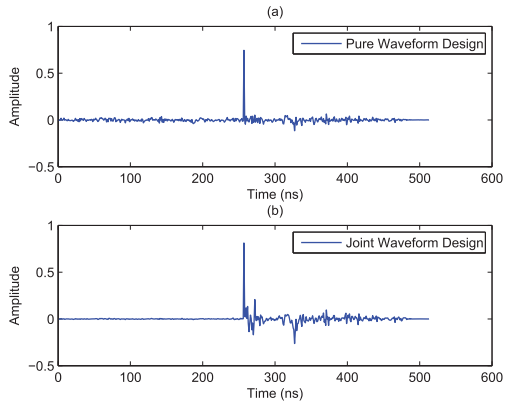

Fig. 5. Equivalent channels for pure waveform design and joint waveform design.

V. NUMERICAL SIMULATION

In this section, we perform numerical simulation to study the performance of the proposed waveform design. The Saleh-Valenzuela channel model for indoor environment is adopted to generate the instances of a multipath channel impulse response. In the S.-V. channel model with 500 MHz sampling rate, the average channel length is around 249. In the following, we denote the waveform design without interference pre-cancellation as *pure waveform design*, and denote the proposed waveform design with interference pre-cancellation as *joint waveform design*. In Figure 5, we plot the equivalent channels, $(\mathbf{g} * \mathbf{h})$, i.e., the composite effect of the transmit waveform and the channel impulse response. Figure 5(a) shows the equivalent channel of using pure waveform design, and Figure 5(b) shows the equivalent channel of using the proposed waveform design. Since the proposed waveform design only suppresses the anti-causal interference and the causal part is compensated by the feedback filter, we can see that the causal interference is untamed and significantly larger than the pure waveform design in Figure 5(a). However, with the same degrees of freedom, the proposed waveform design only needs to suppress about half of the interference compared to the pure waveform design, and it is able to achieve higher peak amplitude and better interference suppression for the anti-causal interference.

Figure 6 and 7 show the single-user BER performance for different waveform design schemes when $D = 1$ and $D = 3$, respectively. Basic TR denotes the traditional TR waveform, which is the time-reversed and conjugated version of the channel impulse response. It can be seen that the joint waveform design can achieve a remarkable performance gain at high SNR region for $D = 1$ compared to $D = 3$. This is because when D is smaller, i.e., the symbol rate is higher, and when the signal power is more dominant than the noise power, the interference is more severe and the joint design has a substantial advantage under such a scenario. The theoretical analysis of the BER performance for the proposed joint design with $D = 1$ is quite close to the simulated result. The theoretical BER of $D = 1$ is more accurate than $D = 3$ due to the fact that the analysis is greatly based on the assumption of a Gaussian distributed interference, and a smaller rate back-off factor results in more interfering multipaths, which makes the

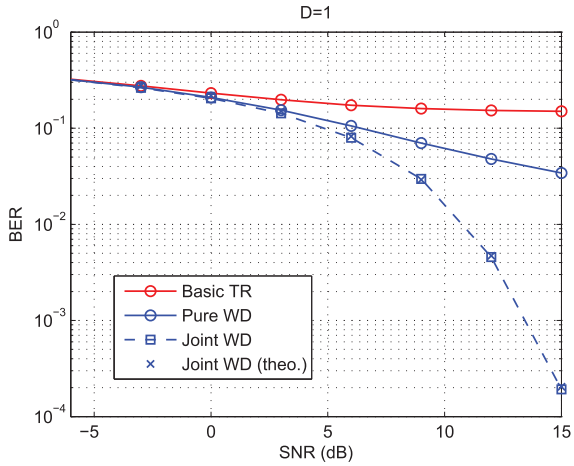

Fig. 6. BER performance comparison of the basic TR, the pure waveform design and the proposed joint waveform design for $D = 1$ with S.-V. channel model of indoor environment where on average $L = 249$.

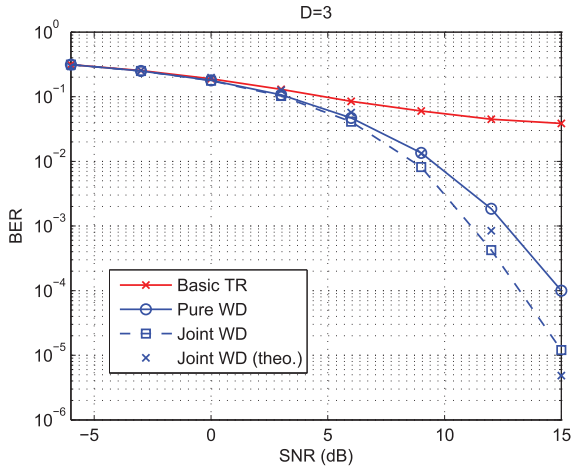

Fig. 7. BER performance comparison of the basic TR, the pure waveform design and the proposed joint waveform design for $D = 3$ with S.-V. channel model of indoor environment where on average $L = 249$.

distribution of the ISI more similar to a Gaussian one. Note that in our previous work [8], the objective is to maximize the sum rate, and thus it may not be fair to compare it with the proposed joint design, which is based on minimizing the sum MSE with interference pre-cancellation. The pure WD, i.e., the waveform design without interference pre-cancellation for minimizing sum MSE, may be a better candidate for performance comparison.

A typical convergence behavior of the two proposed iterative algorithms is plotted in Figure 8 with $K = 2$, $D = 2$ and $P_{\max}/P_N = 18$ dB. The average number of convergence for the proposed alternating optimization algorithm is 10.34 at 0 dB and 26.88 at 18 dB. For the proposed gradient method, the average number of iterations is 7.49 at 0 dB and 48.51 at 18 dB. When $P_{\max}/P_N$ is low, the noise power dominates the interference power, and thus the waveform calculation is easier since a user's waveform should be close to the basic time-reversal waveform which is based its own channel and irrelevant to others'. On the other hand, when the noise power

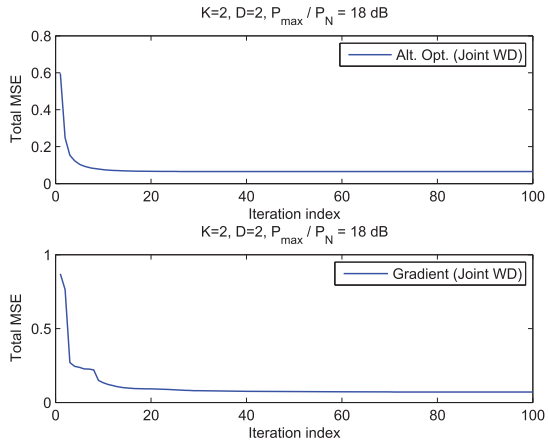

Fig. 8. Convergence behavior of the two proposed iterative algorithms.

is low, the severe ISI and IUI greatly influence the performance, and a user's waveform has to take into account others' waveforms to avoid the interference. Therefore, high $P_{\max}/P_N$ region typically requires more iterations for the algorithms to converge.

For both the alternating optimization algorithm and the gradient algorithm, the ordering of users has to be determined first. As discussed in Section IV, finding the optimal ordering requires an exhaustive search. Heuristic algorithms for finding a suboptimal user ordering, such as the ones in [36], [37], can be adopted. Let us consider the initial step in the alternating optimization algorithm, the α_k's are initialized to be the same, and by substituting the solutions of $\mathbf{g}_k$'s into the MSE in (22), the resulting total MSE is given by

$$\sum_{k=1}^{K} \mathrm{MSE}_k = \sum_{k=1}^{K} P_V \left(1 - \mathbf{h}_{\pi_k L_D} \mathbf{T}_{\pi_k}^{-1} \mathbf{h}_{\pi_k L_D}\right), \qquad (31)$$

where

$$\mathbf{T}_{\pi_k} = \sum_{j \le k} \mathbf{h}_{\pi_j L_D} \mathbf{h}_{\pi_j L_D}^H + \sum_{j=1}^{K} \sum_{l=1}^{L_D} \mathbf{h}_{\pi_j l} \mathbf{h}_{\pi_j l}^H + \frac{P_N}{P_V} \mathbf{I}. \qquad (32)$$

We consider a greedy algorithm exploiting the fact that $\mathbf{T}_{\pi_k}$ does not depend on the particular ordering of $\{\pi_j, j \le k\}$ for the first term in (32) and the second term is the sum of all users' causal ISI and does not rely on the overall ordering. Based on this, once $\{\pi_j, j > k\}$ is determined, MSE_k can be optimized by choosing π_k. We can sequentially choose $\pi_K, \ldots, \pi_1$, i.e., the greedy $\{\pi_k^{\mathrm{G}}\}$ can be determined by

$$\pi_k^{\mathrm{G}} = \arg \max_{\pi_k \notin \{\pi_j^{\mathrm{G}}, j > k\}} \mathbf{h}_{\pi_k L_D} \mathbf{T}_{\pi_k}^{-1} \mathbf{h}_{\pi_k L_D},$$
$$\text{for } k = K, K-1 \ldots, 1. \qquad (33)$$

However, such a greedy approach is not globally optimal since first of all, the objective function in (31) is an approximation since we assume $\{\alpha_k\}$ the same, and secondly, even if the globally optimal $\{\pi_j, j > k\}$ can be found, the subsequent global optimization of π_k has to take into account all terms in (31)

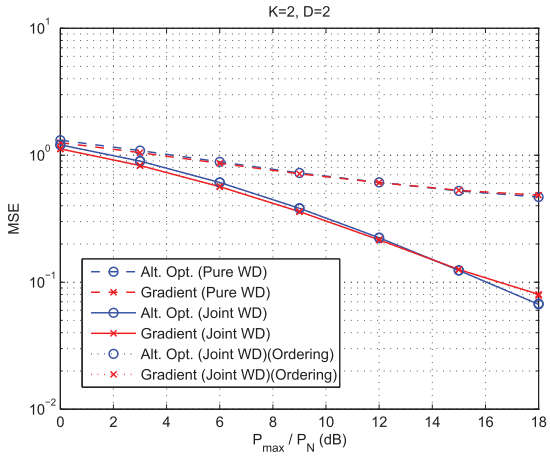

Fig. 9. Total MSE performance comparison of the alternating optimization method and the gradient method for $K = 2$ and $D = 2$ with S.-V. channel model of indoor environment where on average $L = 249$.

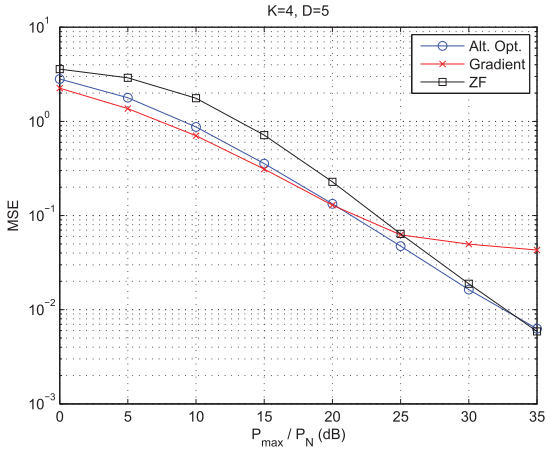

Fig. 11. Total MSE performance comparison of the alternating optimization method, the gradient method, and the ZF technique for $K = 4$ and $D = 5$ with Gaussian channel model of $L = 40$.

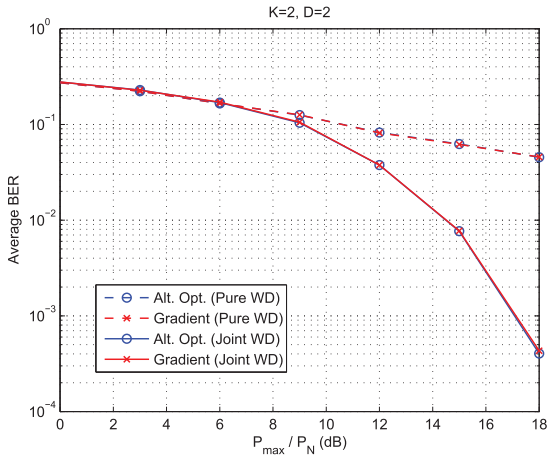

Fig. 10. Average BER performance comparison of the alternating optimization method and the gradient method for $K = 2$ and $D = 2$ with S.-V. channel model of indoor environment where on average $L = 249$.

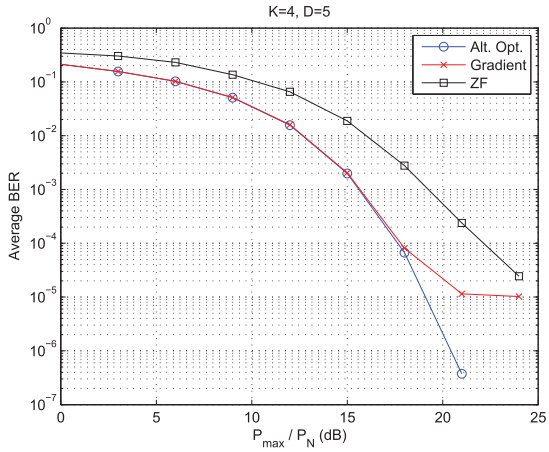

Fig. 12. Average BER performance comparison of the alternating optimization method, the gradient method, and the ZF technique for $K = 4$ and $D = 5$ with Gaussian channel model of $L = 40$.

instead of only $\mathbf{h}_{\pi_k L_D}\mathbf{T}_{\pi_k}^{-1}\mathbf{h}_{\pi_k L_D}$, but such optimization is quite involved and does not permit a better solution other than the exhaustive search.

In Figure 9 and 10, we compare the total MSE and the average BER performance of the methods with $K = 2$ and $D = 2$. It can be seen that for the total MSE, the alternating optimization algorithm performs slightly better than the gradient method at high power region while it performs a bit worse at low power region. However, such a difference does not appear obvious in the average BER performance. The greedy ordering algorithm does not show any perceivable advantage since the current symbols only contribute a small portion to the total interference.

In Figures 11 and 12, we compare the proposed algorithms with the zero-forcing (ZF) technique, which is well-known in MIMO beamforming design and often considered as a benchmark in the high SNR regime. For the sake of benchmarking, the S.-V. channel model is replaced with a simpler model, i.e., the channel coefficients are i.i.d. Gaussian distributed with variance $1/L$, where the channel length $L = 40$, the number of users $K = 4$ and the rate back-off factor $D = 5$. The ZF waveform is computed by $\mathbf{g}_k^{\mathrm{ZF}} = c^{\mathrm{ZF}}\mathbf{H}_{\mathrm{anti},k}^{\dagger}\mathbf{e}_0$, where $\mathbf{H}_{\mathrm{anti},k}$ denotes the matrix composed of the anti-causal interference, $\{\mathbf{h}_{jl}^H | j = 1, \ldots, K; l = 1, \ldots, L_D - 1\}$ and $\{\mathbf{h}_{jL_D}^H | j < k\}$, as its rows, and the last row of $\mathbf{H}_{\mathrm{anti},k}$ is $\mathbf{h}_{kL_D}$. The operator $(\cdot)^{\dagger}$ denotes the Moore-Penrose pseudo inverse, the vector $\mathbf{e}_0$ denotes a vector with the last element being 1 and other elements are zeros, and c^{ZF} is a scalar for power normalization. The receiver gain $\alpha_k^{\mathrm{ZF}} = (\mathbf{h}_{kL_D}^H\mathbf{g}_k^{\mathrm{ZF}})^*/(|\mathbf{h}_{kL_D}^H\mathbf{g}_k^{\mathrm{ZF}}|^2 + P_N/P_V)$ is obtained by omitting the anti-causal interference and optimizing the MSE. This ZF waveform design ignores the noise power and focuses on minimizing the anti-causal interference that cannot be handled by the interference pre-cancellation technique. From Figure 11, it can be seen that at very high SNR (more than 33 dB), the ZF performs the best among the 3 designs in total MSE. However, in Figure 12, the alternating optimization method outperforms the other 2 methods at the high power region. Interestingly, the advantage of the ZF in total MSE does not carry over to the BER performance. The proposed alternating optimization method, even with the sub-optimality in total MSE, can still achieve a superior performance in BER

compared with the ZF technique. ZF imposes a stricter constraint, which seeks to eliminate all the anti-causal interference by choosing the waveform $\mathbf{g}_k$ from the space that minimizes the anti-causal interference, and this may suffer from reducing the intended signal strength. The proposed algorithms do not have such a constraint and are able to strike a balance between suppressing the anti-causal interference and enhancing the intended signal strength. For both the total MSE and the average BER performance at high power region, the alternating optimization shows a noticeable advantage over the gradient algorithm. At low power region, the total MSE performance of the gradient method is slightly superior than the alternating optimization algorithm, but such a difference is imperceptible in the average BER performance.

At high SNR, the gradient algorithm appears to have a floor and performs worse than the alternating optimization algorithm in the average BER performance. This is not always true for each individual channel realization, but a statistical performance. We believe that this performance difference is due to how the algorithms tackle the non-convexity of the optimization problem. Both algorithms aim to search for a local optimum. The gradient algorithm transforms the optimization problem into a function of $\{\mathbf{g}_k\}$ by removing the dependency of $\{\alpha_k\}$. Such a transformation may result in a highly non-linear function in terms of $\{\mathbf{g}_k\}$, which could lead to a worse solution if the search is trapped in a worse local optimum. The alternating optimization algorithm, on the other hand, considers this non-convex problem as two entangled convex problems, where the global optimum of each problem can be efficiently found if the solution to the other problem is given. We believe that the alternating optimization algorithm performs better since it takes advantage of the special problem structure, i.e., it utilizes more information than the gradient algorithm.

As to the high-SNR slopes, it is worth noting that there is no guarantee that the slope of the ZF technique in general is worse than that of the alternating optimization algorithm since the high-SNR slope reflects the degrees of freedom of the equivalent channel, which are not necessarily be degraded by the ZF waveforms. Thus, it is possible that the high-SNR slope of the alternating optimization algorithm turns out to be the same or better than that of the ZF technique at higher SNR than showed in the figures.

In Figure 13, the proposed interference pre-cancellation technique is compared with the basic TR waveform and the pure waveform design for the robustness to channel uncertainty. The channel uncertainty model for the k-th user's channel is given by $\hat{\mathbf{h}}_k = \mathbf{h}_k + \mathbf{e}_k$, where $\hat{\mathbf{h}}_k$ denotes the estimated channel vector, $\mathbf{h}_k$ denotes the true channel with variance σ_h^2 for each element, and $\mathbf{e}_k$ is the estimation error with variance σ_e^2 for each element. It can be observed that the proposed technique performs the best among the three for most of the channel uncertainty region $(\sigma_e^2/(\sigma_e^2+\sigma_h^2) < 0.82)$. Comparing with the pure waveform design, the basic TR waveform is more robust when the uncertainty is high. When the channel uncertainty is very severe, the basic TR waveform is slightly more robust than the others. However, in such a scenario, none of the three waveforms are usable since the BER is close to 0.5.

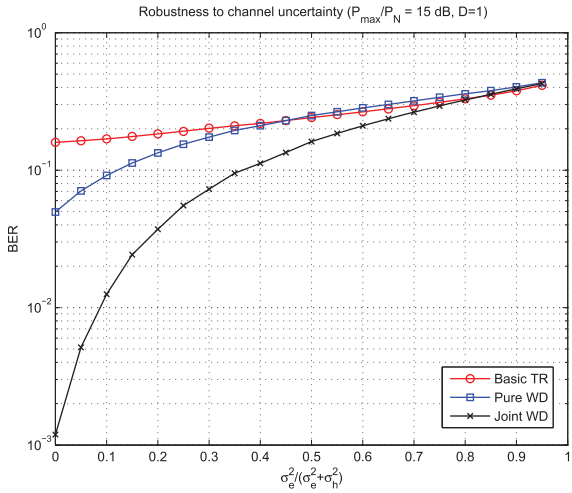

Fig. 13. Comparison of the basic TR, the pure waveform design and the proposed joint waveform design for BER versus channel uncertainty.

The spatial focusing performance of the proposed technique can also be inferred from Figure 13. As the spatial distance increases, the channel correlation between the two locations decreases, and thus the channel uncertainty is higher. The BER performance versus spatial distance is expected to be similar to the trend in Figure 13. Therefore, we can infer that the spatial focusing performance of the proposed interference pre-cancellation technique is superior than the basic TR waveform.

VI. Conclusion

In this work, we proposed the waveform design with interference pre-cancellation for wideband communication systems such as TR systems by exploiting the symbol information available at the transmitter. It was shown that the optimal waveform design with interference pre-cancellation is to compensate the causal interference by a feedback filter and to suppress the anti-causal interference using the waveform. For the multi-user scenario, the causality of both ISI and IUI determines its similar role in the joint design. The resulting multi-user waveform design is a non-convex optimization problem, for which we proposed two iterative algorithms, including an alternating optimization algorithm and a gradient method. Both algorithms can be guaranteed to converge to sub-optimal solutions. For both the total MSE and the average BER performance at high power region, the alternating optimization shows a noticeable advantage over the gradient algorithm. At low power region, the total MSE performance of the gradient method is slightly superior than the alternating optimization algorithm, but such a difference is imperceptible in the average BER performance. Simulation results were shown to validate the convergence of the proposed algorithms and demonstrate the effectiveness of the proposed joint design, especially in the high interference regime. As possible future extensions, applications of the proposed joint design to the multi-antenna scenarios can be attained by utilizing the idea of compensating the causal interference and suppressing the anti-causal interference.

REFERENCES

[1] B. Wang, Y. Wu, F. Han, Y.-H. Yang, and K. J. R. Liu, "Green wireless communications: A time-reversal paradigm," *IEEE J. Sel. Areas Commun.*, vol. 29, no. 8, pp. 1698–1710, Sep. 2011.

[2] F. Han, Y.-H. Yang, B. Wang, Y. Wu, and K. J. R. Liu, "Time-reversal division multiple access over multi-path channels," *IEEE Trans. Commun.*, vol. 60, no. 7, pp. 1953–1965, Jul. 2012.

[3] M. Fink, "Time reversal of ultrasonic fields. I. Basic principles," *IEEE Trans. Ultrason., Ferroelectr., Freq. Control*, vol. 39, no. 5, pp. 555–566, Sep. 1992.

[4] C. Oestges, A. Kim, G. Papanicolaou, and A. Paulraj, "Characterization of space-time focusing in time-reversed random fields," *IEEE Trans. Antennas Propag.*, vol. 53, no. 1, pp. 283–293, Jan. 2005.

[5] J. Proakis and M. Salehi, *Digital Communications*, 5th ed. New York, NY, USA: McGraw-Hill, 2008.

[6] Y. Chen *et al.*, "Time-reversal wireless paradigm for green Internet of Things: An overview," *IEEE Internet Things J.*, vol. 1, no. 1, pp. 81–98, Feb. 2014.

[7] M. Emami, M. Vu, J. Hansen, A. Paulraj, and G. Papanicolaou, "Matched filtering with rate back-off for low complexity communications in very large delay spread channels," in *Proc. 38th Asilomar Conf. Signals Syst. Comput.*, 2004, pp. 218–222.

[8] Y.-H. Yang, B. Wang, W. S. Lin, and K. J. R. Liu, "Near-optimal waveform design for sum rate optimization in time-reversal multiuser downlink systems," *IEEE Trans. Wireless Commun.*, vol. 12, no. 1, pp. 346–357, Jan. 2013.

[9] Z. Ahmadian, M. Shenouda, and L. Lampe, "Design of pre-rake DS-UWB downlink with pre-equalization," *IEEE Trans. Commun.*, vol. 60, no. 2, pp. 400–410, Feb. 2012.

[10] Y. Jin, J. M. Moura, and N. O'Donoughue, "Adaptive time reversal beamforming in dense multipath communication networks," in *Proc. 42nd Asilomar Conf. Signals Syst. Comput.*, Oct. 2008, pp. 2027–2031.

[11] R. C. Daniels and R. W. Heath, "Improving on time-reversal with MISO precoding," in *Proc. 8th Int. Symp. Wireless Pers. Commun. Conf.*, Aalborg, Denmark, 2005, pp. 18–22.

[12] P. Kyritsi, G. Papanicolaou, P. Eggers, and A. Oprea, "Time reversal techniques for wireless communications," in *Proc. IEEE Veh. Technol. Conf.*, 2004, pp. 47–51.

[13] M. Brandt-Pearce, "Transmitter-based multiuser interference rejection for the downlink of a wireless CDMA system in a multipath environment," *IEEE J. Sel. Areas Commun.*, vol. 18, no. 3, pp. 407–417, Mar. 2000.

[14] W. H. Gerstacker, R. R. Müller, and J. B. Huber, "Iterative equalization with adaptive soft feedback," *IEEE Trans. Commun.*, vol. 48, no. 9, pp. 1462–1466, Sep. 2000.

[15] M. H. M. Costa, "Writing on dirty paper," *IEEE Trans. Inf. Theory*, vol. IT-29, no. 3, pp. 439–441, May 1983.

[16] C. Windpassinger, R. F. H. Fischer, T. Vencel, and J. Huber, "Precoding in multiantenna and multiuser communications," *IEEE Trans. Wireless Commun.*, vol. 3, no. 4, pp. 1305–1316, Jul. 2004.

[17] W. Yu, D. Varodayan, and J. Cioffi, "Trellis and convolutional precoding for transmitter-based interference presubtraction," *IEEE Trans. Commun.*, vol. 53, no. 7, pp. 1220–1230, Jul. 2005.

[18] S. Shi, M. Schubert, and H. Boche, "Downlink MMSE transceiver optimization for multiuser MIMO systems: Duality and sum-MSE minimization," *IEEE Trans. Signal Process.*, vol. 55, no. 11, pp. 5436–5446, Nov. 2007.

[19] M. B. Shenouda and T. N. Davidson, "A framework for designing MIMO systems with decision feedback equalization or Tomlinson-Harashima precoding," *IEEE J. Sel. Areas Commun.*, vol. 26, no. 2, pp. 401–411, Feb. 2008.

[20] C. Hellings, M. Joham, and W. Utschick, "Gradient-based power minimization in MIMO broadcast channels with linear precoding," *IEEE Trans. Signal Process.*, vol. 60, no. 2, pp. 877–890, Feb. 2012.

[21] M. Tomlinson, "New automatic equaliser employing modulo arithmetic," *Electron. Lett.*, vol. 7, no. 5, pp. 138–139, 1971.

[22] M. Miyakawa and H. Harashima, "A method of code conversion for a digital communication channel with intersymbol interference," *Trans. Inst. Electron. Commun. Eng. Japan*, vol. 52, pp. 272–273, 1969.

[23] F. Han and K. J. R. Liu, "A multiuser TRDMA uplink system with 2D parallel interference cancellation," *IEEE Trans. Commun.*, vol. 62, no. 3, pp. 1011–1022, Mar. 2014.

[24] S. Boyd and L. Vandenberghe, *Convex Optimization*. Cambridge, U.K.: Cambridge Univ. Press, 2004.

[25] P. Kyritsi, P. Stoica, G. Papanicolaou, P. Eggers, and A. Oprea, "Time reversal and zero-forcing equalization for fixed wireless access channels," in *Proc. 39th Asilomar Conf. Signals Syst. Comput.*, 2005, pp. 1297–1301.

[26] D. Guo, S. Shamai, and S. Verdu, "Mutual information and minimum mean-square error in Gaussian channels," *IEEE Trans. Inf. Theory*, vol. 51, no. 4, pp. 1261–1282, Apr. 2005.

[27] S. Zohar, "Toeplitz matrix inversion: The algorithm of WF Trench," *J. ACM (JACM)*, vol. 16, no. 4, pp. 592–601, 1969.

[28] H. Sakai, "Circular lattice filtering using Pagano's method," *IEEE Trans. Acoust. Speech Signal Process.*, vol. SSP-30, no. 2, pp. 279–287, Apr. 1982.

[29] R. Wesel and J. Cioffi, "Achievable rates for Tomlinson-Harashima precoding," *IEEE Trans. Inf. Theory*, vol. 44, no. 2, pp. 824–831, Mar. 1998.

[30] L. Sanguinetti and M. Morelli, "Non-linear pre-coding for multiple-antenna multi-user downlink transmissions with different QoS requirements," *IEEE Trans. Wireless Commun.*, vol. 6, no. 3, pp. 852–856, Mar. 2007.

[31] A. D'Amico and M. Morelli, "Joint Tx-Rx MMSE design for MIMO multicarrier systems with Tomlinson-Harashima precoding," *IEEE Trans. Wireless Commun.*, vol. 7, no. 8, pp. 3118–3127, Aug. 2008.

[32] W. Yu, D. P. Varodayan, and J. M. Cioffi, "Trellis and convolutional precoding for transmitter-based interference presubtraction," *IEEE Trans. Commun.*, vol. 53, no. 7, pp. 1220–1230, Jul. 2005.

[33] G. D. Forney Jr., "Trellis shaping," *IEEE Trans. Inf. Theory*, vol. 38, no. 2, pp. 281–300, Mar. 1992.

[34] K. Takeda, H. Tomeba, and F. Adachi, "Theoretical analysis of joint THP/pre-FDE for single-carrier signal transmissions," in *Proc. IEEE Wireless Commun. Netw. Conf. (WCNC)*, 2009, pp. 1–6.

[35] E. C. Peh and Y.-C. Liang, "Power and modulo loss tradeoff with expanded soft demapper for LDPC coded GMD-THP MIMO systems," *IEEE Trans. Wireless Commun.*, vol. 8, no. 2, pp. 714–724, Feb. 2009.

[36] A. Mezghani, R. Hunger, M. Joham, and W. Utschick, "Iterative THP transceiver optimization for multi-user MIMO systems based on weighted Sum-MSE minimization," in *Proc. 7th IEEE Workshop Signal Process. Adv. Wireless Commun. (SPAWC)*, Dec. 2006, pp. 1–5.

[37] A. Mezghani, R. Ghiat, and J. A. Nossek, "Transmit processing with low resolution D/A-converters," in *Proc. 16th IEEE Int. Conf. Electron. Circuits Syst. (ICECS)*, Dec. 2009, pp. 683–686.

Yu-Han Yang (S'06) received the B.S. degree in electrical engineering, and the M.S. degrees (two) in computer science and communication engineering from National Taiwan University, Taipei, Taiwan, in 2004 and 2007, respectively, and the Ph.D. degree from the University of Maryland, College Park, College Park, MD, USA, in 2013. Currently, he is with Google Inc., Mountain View, CA, USA. His research interests include wireless communications and signal processing. He was the recipient of Jimmy H. C. Lin Invention Award from the ECE Department, University of Maryland in 2013. He was also the recipient of the Study Abroad Scholarship from Taiwan (R.O.C.) Government from 2009 to 2010.

K. J. Ray Liu (F'03) was named a Distinguished Scholar-Teacher of University of Maryland, College Park, College Park, MD, USA, in 2007, where he is Christine Kim Eminent Professor of Information Technology. He leads the Maryland Signals and Information Group conducting research encompassing broad areas of information and communications technology with recent focus on future wireless technologies, network science, and information forensics and security. He was the recipient of the 2016 IEEE Leon K. Kirchmayer Technical Field Award on graduate teaching and mentoring, the IEEE Signal Processing Society 2014 Society Award, and the IEEE Signal Processing Society 2009 Technical Achievement Award. Recognized by Thomson Reuters as a Highly Cited Researcher, he is a Fellow of AAAS. He was the President of the IEEE Signal Processing Society, where he has served as Vice President—Publications and Board of Governor. He has also served as the Editor-in-Chief of the *IEEE Signal Processing Magazine*. He also received teaching and research recognitions from University of Maryland including university-level Invention of the Year Award; and college-level Poole and Kent Senior Faculty Teaching Award, Outstanding Faculty Research Award, and Outstanding Faculty Service Award, all from A. James Clark School of Engineering.